1995

Vehicle Control for Automated Highway Systems for Improved Lateral Maneuverability

Pushkin Kachroo
University of Nevada, Las Vegas, pushkin@unlv.edu

M. Tomizuka
Virginia Polytechnic Institute and State University

Vehicle Control for Automated Highway Systems For Improved Lateral Maneuverability

Pushkin Kachroo
Center for Transportation Research
Virginia Polytechnic Institute and State University
Blacksburg, VA 24061-0536

Masayoshi Tomizuka
Department of Mechanical Engineering
University of California at Berkeley
Berkeley, California 94720

Abstract

In this paper, longitudinal and lateral vehicle control for Automated Highway Systems (AHS) are studied together for their coupling effects. It is shown that longitudinal controllers which directly control the wheel slip are inherently more stable, especially during lateral maneuvers on very slippery road conditions, than longitudinal controllers which do not take wheel slip into account.

1. INTRODUCTION

For highway automation of vehicles a complete motion control strategy incorporating both longitudinal and lateral control algorithms must be designed. This paper describes how to integrate longitudinal traction control with lateral control. Active traction control is important not only for longitudinal motion but also for producing a desirable lateral response. Since wheel slip has an important influence over longitudinal as well as lateral tractive forces, longitudinal traction control, which regulates the wheel slip at commanded values, can be used to affect the lateral performance of a vehicle. Specifically, on an icy section of a curved path, traction control can be used to maintain a high lateral tractive force by keeping control over the wheel slip. It is more difficult to control vehicles on icy curved paths using passive (tractionless) controllers, since they do not regulate wheel slip.

A nonlinear bicycle model of the vehicle [1] is briefly introduced in this paper to explain the essential dynamics of the overall system. This model has five degrees of freedom- three degrees for longitudinal motion, and two degrees for lateral motion. The lateral dynamics are characterized by the yaw rate and the lateral velocity, whereas the longitudinal motion dynamics are characterized by the longitudinal velocity and the front and rear wheel angular velocities. The longitudinal controller is designed using sliding mode principles. The lateral nonlinear dynamics are linearized about some nominal operating conditions in order to facilitate the design of a linear control law. The frequency-shaped linear quadratic (FSLQ) control theory is used to design the lateral feedback controller. By using this design theory, the ride quality can be included in the performance index explicitly. Meanwhile, the high-frequency robustness characteristic can be improved by properly choosing the weighting factors of the performance index.

2. MODELING

Two models are described for the vehicle system. A five degrees of freedom nonlinear model is introduced first to represent the essential dynamics of the system. A simplified lateral dynamics model is obtained by linearizing the nonlinear model and retaining the lateral and yaw motion dynamics. The longitudinal feedback law is based on the sliding mode longitudinal traction control of the previous paper . The lateral feedback controller is designed using the simplified model. The performance evaluations are based on simulations performed on the nonlinear model. Both models can describe four-wheel-steering, four-wheel-drive vehicles. However, in this paper they are used for front-wheel-steering, four-wheel-drive vehicles only. We have considered four wheel drive instead of two wheel drive in this paper , because four wheel drive is a more generalized case. The mathematical model for a two wheel case can be easily derived from a four wheel model by ignoring the longitudinal friction terms on the two non-driving wheels. Although, in this paper , the simulations are performed for four wheel drive vehicle, the control design is very similar for the two wheel drive.

A. Nonlinear Vehicle Model

Free body diagram of the vehicle model is shown in Figure 1. The nonlinear bicycle model of the vehicle, described here, is adopted from Taheri [1]. This model has five degrees of freedom: longitudinal and lateral velocities, yaw rate, and rotational velocities for the front and rear wheels. Although this model is described for the acceleration case only, it can be easily modified for the deceleration case. Since, Taheri and Law's description in [1] is concise and suits for the purpose of the present study, Appendix A in [1] is inserted below, with the addition of wind disturbance.

The lateral components of the forces of the roads on the tires are F_{yf} and F_{yr}, the longitudinal components are F_{xf} and F_{xr}, where the f and r subscripts refer to front and rear, respectively. The longitudinal wind thrust is F_{wx}, and the lateral wind thrust is F_{wy}. The effects of camber and self aligning moments are neglected. Summing the lateral forces along the body y axis leads to

$$F_{yf}\cos\delta_f + F_{xf}\sin\delta_f + F_{yr}\cos\delta_r + F_{xr}\sin\delta_r + F_{wy} = M_v(\dot{v}_y + v_x r) \quad (1)$$

where, M_v is the vehicle mass, V_x and V_y are the longitudinal and lateral components (on body axis) of the vehicle velocity, and r is the yaw rate. The angles δ_f and δ_r are the front and rear wheel steering angles. Summing the longitudinal forces along the body x axis gives

$$F_{xf}\cos\delta_f - F_{yf}\sin\delta_f + F_{xr}\cos\delta_r - F_{yr}\sin\delta_r - F_{wx} = M_v(\dot{v}_x - v_y r) \quad (2)$$

The sum of the yaw moments about the center of gravity of the vehicle yields

$$L_f(F_{yf}\cos\delta_f + F_{xf}\sin\delta_f) - L_r(F_{yr}\cos\delta_r + F_{xr}\sin\delta_r) = I\dot{r} \quad (3)$$

0-7803-2559-1/95 $4.00 © 1995 IEEE

where, I is the yaw moment of inertia of the vehicle. For the front and rear wheels, the sum of torques about the axle results in

$$T_f - F_{xf} R_w = I_{wf} \dot{\omega}_f \quad (4)$$

$$T_r - F_{xr} R_w = I_{wr} \dot{\omega}_r \quad (5)$$

where, ω_f and ω_r are the angular velocities of the front and rear wheels, I_{wf} is the inertia of the front wheels about the axle, I_{wr} is the inertia of the rear wheels about the axle, R_w is the wheel radius, and T_f and T_r are the applied torques for the front and rear, respectively.

The forces predicted by the tire model depend on the instantaneous value of the road's normal force on the tire. The normal forces change due to the longitudinal acceleration. For the model used, the effects of the suspension system are neglected. Thus, the normal forces on the front and rear tires are obtained by summing moments about the two contact patches. The resulting equations for the total normal reaction for the front tires, N_f, and the total normal reaction for the rear tires, N_r, are

$$N_f = \frac{L_r M_v g}{(L_f + L_r)} \quad (6)$$

$$N_r = \frac{L_f M_v g}{(L_f + L_r)} \quad (7)$$

The nonlinear tire forces are evaluated using the slip angle and the longitudinal slip for each tire. The side slip angle β, is the angle between the vehicle centerline and the velocity vector of the vehicle center of gravity. The tire slip angles are

$$\alpha_f = \delta_f - \tan^{-1}[(v_y + L_f r)/v_x] \quad (8)$$

and,

$$\alpha_r = \delta_r - \tan^{-1}[(v_y - L_r r)/v_x] \quad (9)$$

The values of the longitudinal slip are

$$\lambda_f = (\omega_f R_w - V_{wf})/(\omega_f R_w) \quad (10)$$

$$\lambda_r = (\omega_r R_w - V_{wr})/(\omega_r R_w) \quad (11)$$

where V_{wf} and V_{wr} are the longitudinal components of the velocity of the front and rear axles, respectively,

$$V_{wf} = v_f \cos \alpha_f \quad (12)$$

$$V_{wr} = v_r \cos \alpha_r \quad (13)$$

and the magnitudes of the velocities of the front and rear axles, V_f and V_r are

$$v_f = [(v_y + L_f r)^2 + v_x^2]^{1/2} \quad (14)$$

$$v_r = [(v_y - L_r r)^2 + v_x^2]^{1/2} \quad (15)$$

When the characteristics of the tire (tire pressure, road and tire surface condition, temperature, etc.) are fixed, the traction and turning forces generated from the tire are solely determined by the tire slip angle and the wheel slip (tire slip ratio). The longitudinal tire adhesion coefficient is defined as the ratio of longitudinal tire force and the normal force on the same tire. Similarly, the lateral tire adhesion coefficient is defined as the ratio of the lateral tire force and the normal force on the same tire. These adhesion coefficients are nonlinear functions of slip angle and slip ratio. The longitudinal adhesion coefficient versus the slip ratio curve looks like a serpentine curve which gets flatter and flatter for increasing values of slip angle. On the other hand, the lateral adhesion coefficient versus the slip ration curve resembles a Gaussian curve which gets flatter for decreasing slip angle values. Since the adhesion coefficients are functions of slip ratio and slip angle, they can be represented by three dimensional curves. Figure 2 shows the longitudinal adhesion coefficient on the z-axis, while slip ratio and slip angle are plotted on the x and y axes, respectively. Figure 3 shows the lateral adhesion coefficient on the z-axis, while slip ratio and slip angle are on the x and y axes, respectively. These plots were drawn by using approximate analytical functions for the adhesion coefficient versus wheel slip curves. A mathematical serpentine function was used for the longitudinal adhesion coefficient and a Gaussian function was used for lateral adhesion.

B. Linearized Model for Lateral Control

The model for lateral control includes only the lateral and the yaw motions of the mass center of the vehicle. The derivation of the linearized model, described below, is adapted from the model used by Matsumoto and Tomizuka in [2]. For the sake of linearization, it is assumed that the steering angles are small, so that (1) and (3) can be replaced by

$$\dot{v}_y = [F_{yf} + F_{xf}\delta_f + F_{yr} + F_{xr}\delta_r + F_{wy}]/M_v - v_x r \quad (16)$$

$$\dot{r} = [L_f(F_{yf} + F_{xf}\delta_f) - L_r(F_{yr} + F_{xr}\delta_r)]/I \quad (17)$$

The lateral tire forces F_{yf} and F_{yr} are functions of the lateral road-tire adhesion coefficients μ_{yf} and μ_{yr}, respectively so that

$$F_{yf} = \mu_{yf} N_f \quad (18)$$

$$F_{yr} = \mu_{yr} N_r \quad (19)$$

Lateral road-tire friction is dependent on the road-tire condition and the slip ratio λ_f and λ_r . Furthermore, μ_{yf} and μ_{yr} are approximately proportional to the wheel slip angles α_f and α_r, respectively. Thus, μ_{yf} and μ_{yr} can be described as

$$\mu_f \approx f_f(\lambda_f)\alpha_f \quad (20)$$

$$\mu_r \approx f_r(\lambda_r)\alpha_r \quad (21)$$

where, f_f and f_r are nonlinear functions which depend on the road-tire condition. Hence, the lateral tire forces can be rewritten as

$$F_{yf} = C_f \alpha_f \quad (22)$$

$$F_{yr} = C_r \alpha_r \quad (23)$$

with the cornering stiffnesses originally defined as [3]

$$C_s = \frac{\partial F_y}{\partial \alpha}\Big|_{\alpha = 0} \quad (24)$$

given here by

$$C_f = f_f(\lambda_f) N_f \quad (25)$$

$$C_r = f_r(\lambda_r) N_r \quad (26)$$

For linearization, the slip angles defined by (8) and (9) can be approximated as

$$\alpha_f = \delta_f - [(v_y + L_f r)/v_x] \quad (27)$$

$$\alpha_r = \delta_r - [(v_y - L_r r)/v_x] \quad (28)$$

The lateral tire forces can now be written as

$$F_{yf} = C_f(\delta_f - [(v_y + L_f r)/v_x]) \quad (29)$$

$$F_{yr} = C_r(\delta_r - [(v_y - L_r r)/v_x]) \quad (30)$$

Substituting these in (16) and (17), we obtain the following linear lateral model of the vehicle.

$$\frac{d}{dt}\begin{bmatrix} v_y \\ r \end{bmatrix} = \mathbf{A}\begin{bmatrix} v_y \\ r \end{bmatrix} + \mathbf{B}\begin{bmatrix} \delta_f \\ \delta_r \end{bmatrix} \quad (31)$$

$$\mathbf{A} = \begin{bmatrix} \frac{-P_1}{M_v} & \frac{-P_2}{M_v} - v_x \\ \frac{-P_2}{I} & \frac{-P_3}{I} \end{bmatrix} \quad \mathbf{B} = \begin{bmatrix} \frac{Q_f}{M_v} & \frac{Q_r}{M_v} \\ \frac{L_f Q_f}{I} & \frac{-L_r Q_r}{I} \end{bmatrix}$$

where, P_i and Q_i are

$$P_1 = \frac{C_f + C_r}{v_x},\ P_2 = \frac{C_f L_f - C_r L_r}{v_x},\ P_3 = \frac{C_f L_f^2 + C_r L_r^2}{v_x}$$

$$Q_f = C_f + F_{xf},\ Q_r = C_r + F_{xr}$$

A detailed analysis of this linearized system is shown in Matsumoto and Tomizuka [2].

3. CONTROLLER DESIGN

The controller design for the overall system is decoupled into independent longitudinal and lateral control laws, although their performance is interdependent. The longitudinal control design is based on the nonlinear longitudinal dynamics of the system, and the lateral control design is based on the linearized lateral dynamics of the system. Sliding mode traction control is used for maintaining a pre-specified distance between platoon vehicles, or in general, for maintaining some desired acceleration or deceleration. Lateral control is designed utilizing Frequency Shaped Linear Quadratic (FSLQ) control based on the linearized model of the vehicle lateral motion, which includes lateral deviation and the yaw angle. Since lateral control is designed for nominal conditions, gain scheduling is considered for varying operating conditions. Another way to deal with varying operating conditions would be to use adaptive control. The details of the two controllers used in the simulations are discussed next.

A. Sliding Mode Longitudinal Traction Controller

The longitudinal traction controller is designed as a twin sliding surface mode. In the dynamics (2) for the longitudinal velocity, the input term for the first sliding surface is $(F_{xf} \cos \delta_f + F_{xr} \cos \delta_r)$, which is evaluated from the desired dynamics for the longitudinal velocity. The two terms in the input for the first sliding surface represent the front wheel and the rear wheel components of the longitudinal tractive force. In four wheel drive vehicles, we have the freedom to choose the distribution of the tractive force between the front and the rear wheels. In the present design, we are using equal distribution of the tractive force, which implies that the two terms in the input for the first sliding surface are kept equal to each other. For a two wheel drive vehicle, one of the terms in the input for the first sliding surface would be zero, and hence, all the longitudinal tractive force would be provided by the two driving wheels. From the desired value of the longitudinal tractive forces for the four wheel drive vehicle we are considering, the desired value of the front and rear wheel slips are calculated by inverting the nominal adhesion coefficient versus wheel slip curve for a given side slip angle. These desired values of the wheel slips are used to drive the second sliding mode surface to obtain the needed torque inputs. The details of the sliding mode control design for traction control are shown in [5].

B. FSLQ Lateral Controller

The FSLQ control theory [6, 7] provides a controller design tool for a linear system, based on the minimization of a quadratic performance index, which includes frequency as a parameter. Frequency shaped designs combine the techniques of classical control design and linear quadratic methods to utilize the strengths of each. Hence, combining the two methods in FSLQ provides greater flexibility in the control design.

Peng and Tomizuka have successfully shown the viability of using FSLQ technique to design vehicle lateral controllers for the highway automation, as it relates to PATH [4]. In the lateral control design, there are numerous advantages in using the FSLQ theory. The main advantages, adopted from [4] are listed below:

(1) Frequency dependent weighting factors are placed on tracking error, lateral velocity error, yaw rate error, yaw angle error, lateral acceleration and control effort terms in the performance index to compromise these conflicting objectives.

(2) The weighting factor on the lateral acceleration term can be shaped in the frequency domain to achieve a good ride quality in the frequency range where passengers are sensitive.

(3) The weighting factors on the tracking error terms can be shaped in the frequency domain appropriately to enhance the tracking performance at low frequencies and the robustness of the controller to high frequency measurement noises and unmodeled dynamics.

The lateral feedback controller is designed by minimizing the following performance index:

$$J = \frac{1}{2\pi}\int_{-\infty}^{\infty} [a^*(j\omega)Q_a(j\omega)a(j\omega) + v_r^*(j\omega)Q_v(j\omega)v_r(j\omega) + r_e^*(j\omega)Q_r(j\omega)r_e(j\omega) + v_r^*(j\omega)Q_{iv}(j\omega)v_r(j\omega) + r^*(j\omega)Q_{ir}(j\omega)r(j\omega) + v_r^*(j\omega)Q_{iiv}(j\omega)v_r(j\omega) + \delta_f^*(j\omega)Q_\delta(j\omega)\delta_f(j\omega)]d\omega \quad (32)$$

In Equation (32), a, the difference between the lateral acceleration, $\dot{v}_y$, and its desired value, $\frac{v_x^2}{\rho}$, is expressed as:

$$a = \dot{v}_y - \frac{v_x^2}{\rho} = \dot{v}_r \quad (33)$$

where ρ is the radius of curvature of the road, and v_r is the lateral deviation velocity of the mass center from the reference. The lateral deviation of the vehicle from the center of the lane is obtained by using magnetic markers in the center of the lane. The lateral deviation is differentiated numerically or using hardware to obtain lateral deviation velocity. The first term of the performance index is used to represent the ride quality, the second, third, fourth, fifth and sixth terms are included for tracking capability, and the fifth term represents the control effort. The frequency dependent weighting factors, Q_a, Q_v, Q_r, Q_{iv}, Q_{ir}, Q_{iiv} and Q_δ are designed to produce satisfactory ride quality, high frequency robustness, and desirable transient and steady-state responses.

The ride quality is reflected in the lateral acceleration term of the performing index. Many specifications such as ISO [8] and rms [9] have been developed to express the ride quality in terms of a frequency dependent weighting index on the lateral acceleration. All these specifications can adequately describe the ride quality [10]. In order not to increase the number of augmented states excessively, the weighting factor is chosen as:

$$Q_a = \frac{q_a^2}{1 + \lambda_a^2 \omega^2} \quad (34)$$

The coefficient λ_a determines the weighting on each frequency component in the lateral acceleration to represent the desired ride quality.

High frequency components in the steering input are not desirable as they can deteriorate the ride quality and may excite the unmodeled dynamics of the system. By reducing the gain in the high frequency range, better robustness in that range can be achieved. Hence, Q_v and Q_r are designed as low pass filters.

$$Q_v = \frac{q_v^2}{1 + \lambda_v^2 \omega^2} \quad (35)$$

$$Q_r = \frac{q_r^2}{1 + \lambda_r^2 \omega^2} \quad (36)$$

Weights on the lateral deviation and yaw angle error are

$$Q_{iv} = \frac{q_{iv}^2}{(j\omega)^2} \quad (37)$$

$$Q_{ir} = \frac{q_{ir}^2}{(j\omega)^2} \quad (38)$$

to minimize their DC component. The steady state lateral deviation approaches zero because of the integral action on lateral deviation introduced by Q_{iiv}.

$$Q_{iiv} = \frac{q_{iiv}^2}{(j\omega)^2} \quad (39)$$

The weight on the input term, Q_δ is chosen as a frequency independent coefficient. The coefficients, λ_v and λ_r are tuned to enhance the high frequency robustness of the controller while maintaining good tracking capability. After choosing the values of λ_a, λ_v and λ_r, the values of q_a, q_v, q_r, q_{iv}, q_{ir}, q_{iiv} and Q_δ are adjusted for further tuning. The FSLQ problem can be transformed to a standard LQ problem by introducing augmented state variables, and the gain vector of the feedback controller can be computed by solving a Riccati equation.

If the radius of curvature and preview information of the path is available, feedforward and preview controllers can also be used to improve the lateral control performance[4, 11, 12].

The gain of the feedback controller depends on the longitudinal velocity and the cornering stiffness. The velocity is available as a sensor measurement, and the cornering stiffness can be estimated from the lateral dynamic equation [4].

4. NUMERICAL SIMULATIONS

The simulations are performed on the nonlinear model described in Section 1.1. The inertial parameters are shown in Table 1. Sliding mode controller based on twin sliding surfaces, is employed for longitudinal traction control and FSLQ controller is used for the lateral direction. A simple PID control law is employed for passive control in the longitudinal direction, which is compared with the active traction control provided by the twin surface sliding mode. The longitudinal control law is designed as follows. First, Equation (2) is rewritten as

$$\dot{v}_x = f + u \quad (40)$$

where

$$f = [- F_{yf} \sin \delta_f - F_{yr} \sin \delta_r - F_{wx} + v_y r]/M_v \quad (41)$$

$$\text{and } u = [F_{xf} \cos \delta_f + F_{xr} \cos \delta_r]/M_v \quad (42)$$

Let s_1 be the first sliding surface, defined as

$$s_1 = \dot{\varepsilon} + c_1 \varepsilon \quad (43)$$

where ε is the spacing error; between the vehicle being controlled and the vehicle in front. The spacing error is defined as the difference between the actual distance between the two vehicles and the desired distance between them. When the desired distance between the two vehicles is a constant, $\dot{\varepsilon}$ becomes the velocity error between the vehicle to be controlled and the vehicle in front. From the first sliding surface, we obtain the value of desired ($F_{xf} \cos \delta_f + F_{xr} \cos \delta_r$) using the sliding mode design steps [see Chapter 7 in 13]. In the simulations presented here, four wheel drive is assumed. Four wheel drive is a more generalized case, and the two wheel drive mathematical model and the control law can easily be derived from the model and the control law for the four wheel drive case. In four wheel drive, the desired longitudinal tractive force is divided equally between the front wheels and the rear wheels. Notice that for a two wheel drive only the two driving wheels would provide the longitudinal tractive force. The second sliding surface is defined by equation the difference between the actual angular velocity of the wheel and the desired angular velocity of the wheel to zero. The second sliding surface dynamics for the front wheels is different than that of the rear wheels. The desired wheel slip is obtained by using the nominal longitudinal adhesion versus wheel slip curve. The wheel slip is numerically differentiated to obtain its derivative, which is used in the control law. The steering angles δ_f and δ_r in ($F_{xf} \cos \delta_f + F_{xr} \cos \delta_r$) are known, and therefore, the required front and rear longitudinal adhesion can be calculated by dividing the front and the rear tractive forces by the corresponding nominal normal forces respectively. For the case of front wheel drive, the driving torque would be applied to the front wheels, which consequently would produce the traction force due to wheel slip.

Table 2 shows the values of the lateral controller design parameter values for the simulations. The gains of the FSLQ controller are precomputed as functions of longitudinal velocity and cornering stiffness. The measurement rates are assumed to be 100 Hz. The simulation path is shown in Figure 4. The path is divided into five regions (A, B, C, D and E). Simulations are performed with and without the asphalt and concrete patch and the icy patch. Region A and region E are straight sections, while regions B, C and D are curved sections of the simulation path. The radius of curvature for all the curved sections is 1.5 Km. In regions A and C, the vehicle is commanded to have a longitudinal acceleration of 1 m/s^2 from 20 m/s to 25 m/s and 25 m/s to 35 m/s respectively. Region A is 112.5m long, region B is 750m long, region C is 300m long, region D is 175 m long and region E is more than 6Km long.

First, simulation on the path without the asphalt and concrete and the icy section was performed with active traction control (sliding mode) and lateral control (FSLQ). The longitudinal velocity is followed very closely. The front wheel slip remains below 0.05. The steering commands, lateral deviation and the yaw rate errors are small.

Simulation results of active traction and lateral control on the path with the asphalt and concrete and the icy patch are shown in Figures 5-6. The asphalt and concrete patch starts at 30.5 seconds from the start and lasts for 10 seconds immediately after which, the icy patch starts, which lasts for 9 seconds. In this case also, the longitudinal velocity is followed very closely. Although the slip value is stabilized in the same region as before, the slip value increases up to approximately 0.15. The steering commands, lateral deviation and the yaw rate errors are greater than what they were in the previous case, but still the values are small.

Simulation is performed for passive traction (a fine tuned PID control law) and lateral control on the path with

and without the asphalt and concrete patch and the icy patch. The results with the patches are shown in Figures 7-8. Without the patches, the performance of the passive traction control is satisfactory, but when the two patches are introduced on the test surface, the vehicle becomes unstable. The slip value increases in the icy patch region and stays in the undesirable negative $\mu-\lambda$ slope region. The steering angle input oscillates with a large amplitude and so does the lateral deviation. The yaw rate errors are also large.

These simulations emphasize the importance of longitudinal traction control to the lateral stability of a vehicle.

Parameters	Values
Mass (M_v)	12495 N
Distance to front axle from car cg, L_f	1.0 m
Distance to rear axle from car cg, L_r	1.45 m
Yaw inertia, I	1627 Kg m^2
Wheel inertia, (I_{wf}, I_{wr})	4.07 Kg m^2
Wheel radius, (R_w)	0.33 m
Front cornering stiffness, C_f	30600 N/rad
Rear cornering stiffness, C_r	44374 N/rad
Longitudinal velocity, v_x	25 m/sec

Table 1 System parameters of the simplified model

Parameters	Values
λ_a	1/180
λ_v	1/1000
λ_r	1/1000
q_a	1
q_v	1.75
q_r	1.75
q_{iv}	2
q_{ir}	2
q_{iiv}	0.1
Q_δ	1

Table 2 Lateral controller design parameter values

5. CONCLUSIONS

A nonlinear model of the vehicle system for combined longitudinal and lateral control was discussed. The control design for the overall system was decoupled into independent longitudinal and lateral control laws. Sliding mode design was used for longitudinal traction control and a PID control law was used for longitudinal passive control. The lateral controller was based on FSLQ theory.

In this paper , we have shown the superiority of active control during lateral maneuvers for a platoon of vehicles, in order to relate the results to highway automation.

The simulation results of active and passive longitudinal control with lateral control on a combination of straight and curved sections with and without an icy patch, showed a superior performance of the vehicle under active traction control.

ACKNOWLEDGMENT

This work was performed as part of the PATH Program of the University of California, and "Smart Highway" project of Virginia Dept. of Transportation, in cooperation with the State of California, Business and Transportation Agency, Department of Transportation, and the United States Department of Transportation, Federal Highway Administration.

REFERENCES

[1] S. Taheri, "A Feasibility Study of the Use of a New Nonlinear Control Law for Automobile Anti-lock Braking Systems", *ACC Proceedings*, vol. 2 of 3, 1990.

[2] M. Togai and P. P. Wang, "Analysis of a Fuzzy Dynamic System and Synthesis of its Controller", *Int. J. Man-Machine Studies*, 22, 355-363, 1985.

[3] H. Sakai, "Theoretical and Experimental Studies on the Dynamical Properties of Tyres, Part 1: Review of Theories of Rubber Friction", *Int. J. of Vehicle Design*, Vol.2, No.1, 1981, pp.78-110.

[4] H. Peng and M. Tomizuka, "Vehicle Lateral Control for Highway Automation", *ACC Proceedings*, San Diego., pp. 788-794, 1990.

[5] Pushkin Kachroo, and Masayoshi Tomizuka, Vehicle Traction Control and its Applications. Technical Report UIPRR-94-08, University of California at Berkeley, Institute of Transportation, 1994.

[6] B. D. O Anderson and J. B. Moore,*Optimal Control-Linear Quadratic Methods*, Englewood Cliffs, NJ: Prentice Hall, 1990.

[7] N. Gupta, "Frequency-Shaped Cost Functionals: Extension of Linear-Quadratic-Gaussian Design Method", *J. Guidance and Contr.*, vol. 3, no. 6, pp. 529-535, Nov.-Dec. 1980.

[8] Anonymous, "A Guide to the Evaluation of Human Exposure to Whole Body Vibration", *ISO/DIS 2631*, International Organization for Standardization, New York, 1972.

[9] R. N. Janeway, "Vehicle Vibration Limits to Fit the Passenger", *S.A.E. Journal*, Vol.56, Aug. 1948, pp.48-49.

[10] C. C. Smith, D. Y. McGehee and A. J. Healey, "The Prediction of Passenger Riding Comfort from Acceleration Data", *Trans. of ASME, Journal of Dynamic Systems, Measurement, and Control*, Vol.100, March 1978, pp.34-41.

[11] S. E. Shladover, C. A. Desoer, J. K. Hedrick, M. Tomizuka, J. Walrand, W. B. Zhang, D. Mcmohan, H. Peng, S. Sheikholeslam and N. Mckeowen, "Automatic Vehicle Control Developments in the PATH Program", *IEEE Trans. Vehic. Technol.*, vol. 40, no. 1, pp. 114-130, Feb. 1991.

[12] A. Y. Lee, "A Preview Steering Autopilot Control Algorithm for Four Wheel Steering Passenger Vehicles", *Advanced Automotive Technologies ASME*, pp. 83-98, 1989.

[13] J.-J. E. Slotine and Weiping Li, *Applied Nonlinear Control*, Prentice Hall, New Jersey, 1991.

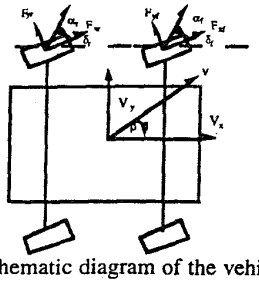

Figure 1 Schematic diagram of the vehicle model for longitudinal and lateral control

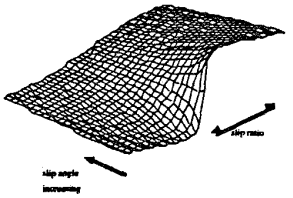

Figure 2 Longitudinal adhesion coefficient versus slip ratio and slip angle

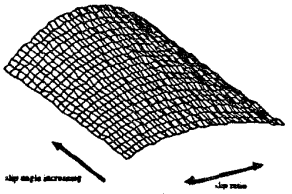

Figure 3 Lateral adhesion coefficient versus slip ratio and slip angle

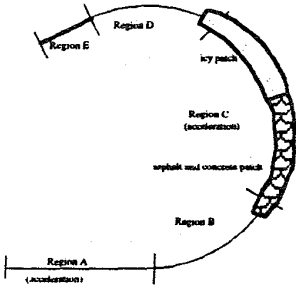

Figure 4 Geometry of the desired trajectory

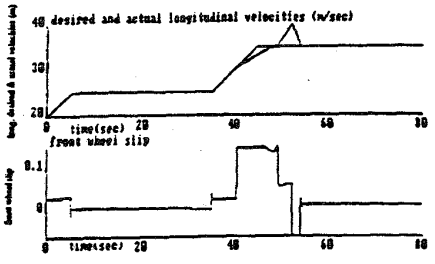

Figure 5 Longitudinal velocity and wheel slip plots for active traction with lateral control

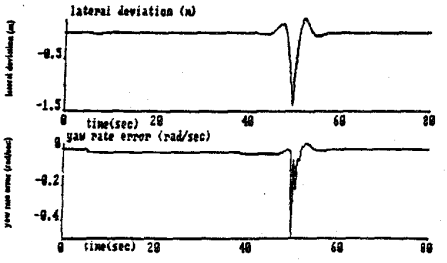

Figure 6 Lateral deviation and yaw rate error plots for activ traction with lateral control

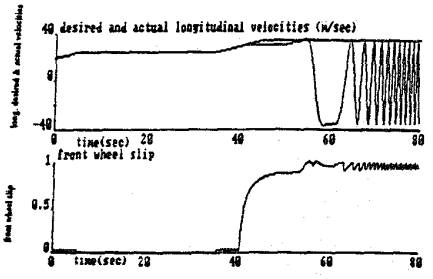

Figure 7 Longitudinal velocity and wheel slip plots for passive traction with lateral control

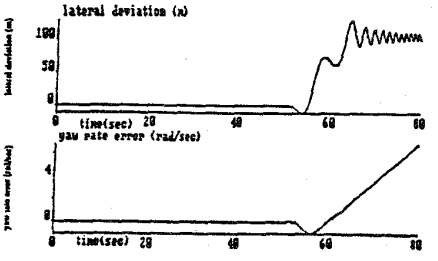

Figure 8 Lateral deviation and yaw rate error plots for passive traction with lateral control